CONSTITUTIVE MODELING OF QUENCH-HARDENABLE BORON STEEL WITH TAILORED PROPERTIES

Tom K. Eller[1,2,*], Lars Greve[1], Michael T. Andres[1], Miloslav Medricky[1], Ansgar Hatscher[1], Timo Meinders[2], Ton van den Boogaard[2]

[1] Volkswagen AG, Group Research, P.O. Box 1777, 38436 Wolfsburg, Germany
[2] University of Twente, P.O. Box 217, 7500 AE Enschede, The Netherlands

ABSTRACT: In this work, a material model is presented that predicts the crash-relevant constitutive behavior of quench-hardenable boron steel 22MnB5 as function of material hardness. Three sets of sheets of 22MnB5 are heat treated such that their as-treated microstructures are close to fully martensitic, bainitic and ferritic/pearlitic, respectively. Hardness measurements show that the resulting blanks cover the full scope of possible hardness values, from 165 HV in the ferritic/pearlitic range to 477 HV in the fully hardened state. These three main grades provide the input data for a constitutive model consisting of an extended Swift hardening law and a strain-based fracture criterion. The hardening behavior of each grade is determined using standard tensile tests. For calibration of the fracture criterion, four different fracture samples are used. The developed model predicts the behavior of intermediate hardness grades by piecewise linear interpolation between the hardening and fracture models of the three calibrated grades. A newly developed tapered tensile test specimen is used to validate the model at hand.

KEYWORDS: Tailored properties, Hot forming, Hardness, Constitutive modeling

1 INTRODUCTION

The hot stamping process is gaining popularity as production method for crash-relevant structural components in vehicles. Due to the high tensile strengths of hot stamped materials, weight reductions are possible while maintaining, or even improving crashworthiness properties. Some crash-critical components, however, are found to benefit from regions of reduced strength and higher ductility. The B-pillar shown in Figure 1 is an example of such a part. For optimal performance in a side crash, the bottom part should show a high energy absorption capacity, while the upper part should ensure a high intrusion resistance [1]. Common methods to produce parts with such "tailored" mechanical properties are: local reduction of the in-die cooling rate through the use of tool materials with varying thermal conductivities or using increased die temperatures (tempered/tailored tooling), or by post tempering fully hardened parts with differential heating in the furnace [2].

To be able to fully exploit the possibilities of these modern hot stamped steels, it is of paramount importance to attain accurate predictive models of their crash response. In the present study, three sets of quench-hardenable boron steel 22MnB5 are heat treated such that their as-treated microstructures cover the full range of hardness values from 165 HV in the soft ferritic/pearlitic state to 477 HV in the fully hardened, martensitic state. These three variants form the corner stones of a hardness dependent constitutive model consisting of an extended Swift hardening law and a strain-based fracture criterion.

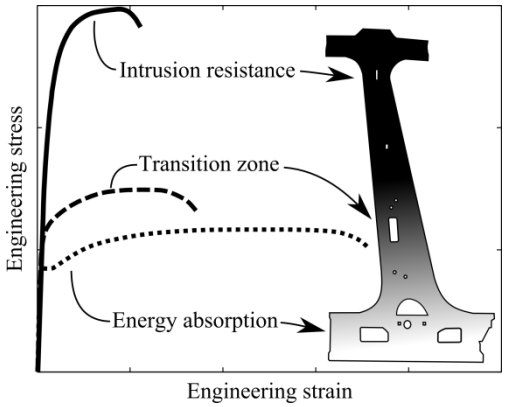

Fig. 1 *Tailored B-pillar with corresponding stress-strain curves.*

2 MATERIAL DESCRIPTION

The material used for this study is 22MnB5. Known by the commercial name Usibor® 1500 P, ArcelorMittal has provided the 22MnB5 steel grade with an aluminum-silicon coating that protects the metal against oxidation and decarburization during the press hardening process [3]. In the

* Corresponding author: 38436 Wolfsburg, P.O. Box 1777, +49 5361 9-41477, tom.karl.eller@volkswagen.de

as-delivered state 22MnB5 has a ferritic/pearlitic microstructure, an ultimate tensile strength of 600 MPa, and a uniform elongation of 0.22. After quenching in cooled stamping tools, a fully martensitic microstructure is obtained resulting in an ultimate tensile strength and uniform elongation of 1500 MPa and 0.06, respectively. The chemical composition of this material is given in Table 1.

Table 1: *Chemical composition of the 22MnB5 used in this work (wt. %) [4].*

C	0.2 – 0.25	Si	0.15 – 0.35
Mn	1.1 – 1.4	Al	≥ 0.015
P	≤ 0.025	Ti	0.02 – 0.05
S	≤ 0.008	B	0.002 – 0.005

3 EXPERIMENTAL WORK

3.1 MATERIAL PREPARATION

In order to create material samples with the desired material hardness, three sets of 22MnB5 sheets were fully austenitized in a furnace at over 900°C, after which they were subjected to carefully controlled cooling processes. The first set of sheets was transferred to a water-cooled stamping tool. It took a total of 11 seconds to take the sheets out of the furnace, transfer them to the press and close it. At first contact with both tool halves, the sheets had cooled down to approximately 700°C. The press, which was cooled to a constant temperature of 25°C, was solely used to ensure good contact between tool surface and sheet, no plastic deformations were applied. After a holding time of 8 seconds, the sheets were removed and left to cool down to room temperature in air. The second set of sheets was transferred to a tempered tool. The same procedure was applied as for the cooled tool sheets, but now with a constant tool temperature of 550°C and a holding time of 14 seconds. The third set of sheets was left inside the furnace to cool down, with the furnace turned off and the door slightly opened.

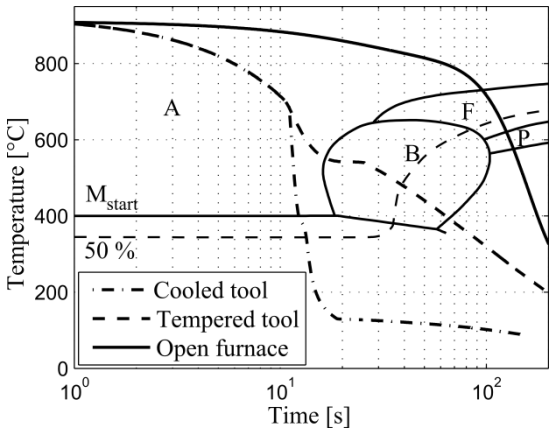

Fig. 2 *Measured cooling curves of the samples superimposed on the CCT diagram of 22MnB5 (CCT data retrieved from [5]).*

The resulting cooling curves are superimposed on the CCT diagram of 22MnB5 and shown in Figure 2. According to the CCT diagram, it seems likely that the cooled tool and open furnace temperature curves result in pure martensite and ferrite/pearlite phase compositions, respectively. The temperature history of the tempered tool sheets indicates that a close to fully bainitic microstructure has been obtained.

3.2 MATERIAL ANALYSIS

The heat treated sheets have been carefully examined with a metallographic analysis and hardness measurements. For this purpose, small samples were cut out of the sheets and mounted in epoxy resin. After several grinding and polishing steps, some samples were used for Vickers hardness tests, and some samples were etched with 3% nital solution and analyzed under a reflected light microscope. The micrographs from the cooled tool sheet showed a fully martensitic microstructure, the corresponding hardness value was found to be 477 HV. The micrographs from the tempered tool sheet revealed that this grade consists of upper bainite with small portions of martensite, which meets the expectations from the CCT diagram in Figure 2. The hardness was found to be 239 HV. Finally, the micrographs from the open furnace sheets showed a fully ferritic/pearlitic microstructure, the hardness was measured to be 163 HV. The results are summarized in Table 2.

The material in the as-delivered state was subjected to the material analysis as well. A fully ferritic/pearlitic microstructure was found with a hardness of 165 HV. The similarities between hardness values and micrographs from the open furnace and the as-delivered material suggest that these two possess the same mechanical properties. Because of the relatively unstable conditions during the cooling process in the open furnace, the material in the as-delivered state will be used for further characterization and will be denoted as ferrite/pearlite grade in the remainder of this work. The tempered tool sheets will be denoted as bainite grade for the sake of simplicity, although small portions of martensite were found. The cooled tool sheets will be denoted as martensite grade.

Table 2: *Results of the Vickers hardness measurements and the metallographic analysis.*

Material grade	**Hardness [HV30]**	**Microstructure**
Cooled tool	477	Martensite
Tempered tool	239	Mainly bainite
Open furnace	163	Ferrite/pearlite
As-delivered	165	Ferrite/pearlite

3.3 Tensile tests

Standard uni-axial tensile tests according to DIN 50125 were performed with the three hardness grades. Quasi-static strain rates of 0.002 s^{-1} were applied. The resulting engineering stress-strain curves are shown in Figure 3. Six tests were done per grade, of which only the ones that fractured inside the range of the extensometer are plotted here. The ferrite/pearlite and the martensite samples show tensile strengths of 600 MPa and 1500 MPa, respectively, which corresponds to the manufacturer specifications for as delivered and fully hardened 22MnB5. The bainite grade has an intermediate tensile strength of 750 MPa.

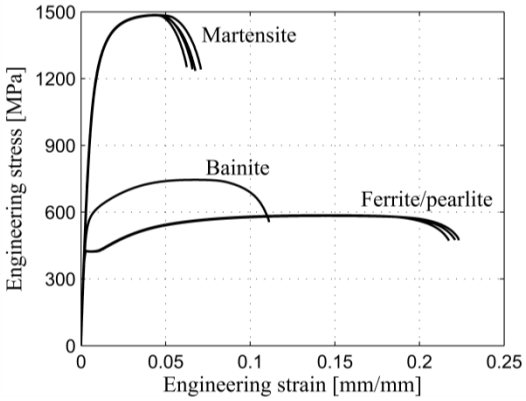

Fig. 3 *Engineering stress/strain results from the standard tensile tests.*

3.4 Fracture tests

Four different fracture tests were carried out for all three 22MnB5 hardness grades in order to collect data for the stress triaxiality and Lode angle dependent modified Mohr-Coulomb fracture criterion [6]. The four fracture specimens were designed such that fracture occurred at locations with well-defined and constant stress states throughout the experiments: uni-axial tension, plane strain tension, simple shear and equibiaxial tension. For a detailed description of specimen geometries, experimental procedures and model calibration, the interested reader is referred to [7]. Here, only the results will be presented, see Section 4.2.

4 Constitutive modeling

4.1 Strain hardening

In order to determine the strain hardening behavior of the three 22MnB5 hardness grades, average curves are extracted from the engineering stress-strain diagram in Figure 3. The engineering stresses and strains are converted to true stresses (σ) and true plastic strains (ε_p):

$$\sigma = \sigma_{eng}\left(1 + \varepsilon_{p,eng}\right) \tag{1}$$

$$\varepsilon_p = \ln\left(1 + \varepsilon_{p,eng}\right) \tag{2}$$

in which $\varepsilon_{p,eng}$ is the plastic engineering strain, calculated by subtracting the elastic strains from the total strains in Figure 3. Equations 1 and 2 can only be used up to the strain at which necking begins. For all three material grades, the converted curves are shown in Figure 4.

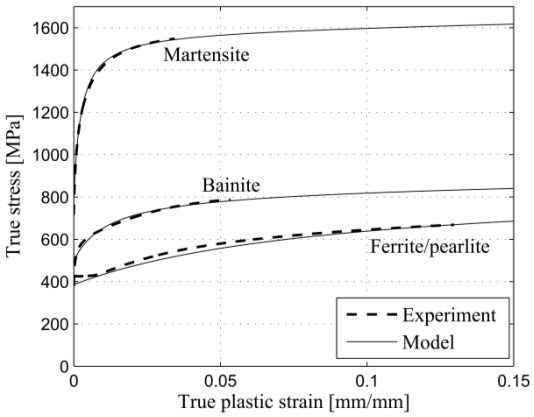

Fig. 4 *True stress-strain curves of the three material grades.*

Looking at Figure 4, it is seen that the ferrite/pearlite grade shows a flat and almost linear strain hardening curve, whereas the martensite curve is characterized by its high curvature at low strains. Due to this variety in shapes, classical hardening laws such as Swift or Voce can be fitted either to the martensitic material or to the ferritic/pearlitic material, but not to both. To overcome this inconvenience, a new extended Swift law is introduced that can be fitted to the full range of 22MnB5 grades:

$$\sigma_y\left(\bar{\varepsilon}_p\right) = k\left(\bar{\varepsilon}_p + \varepsilon_0\right)^n + \frac{p_1\bar{\varepsilon}_p + p_2}{\bar{\varepsilon}_p + p_3} \tag{3}$$

The first term in Equation 3 can be recognized as the Swift hardening equation. The additional rational term brings in extra flexibility at low strains and converges to p_1 for $\bar{\varepsilon}_p \to \infty$. To illustrate the effect of the additional term, Figure 5 shows the best fits of the classical Swift law and the extended Swift law for the martensite grade for small strains. The extended Swift law provides an almost perfect fit, whereas the classical Swift law is unable to approximate the right curvature. A second problem of the classical Swift law, especially for the harder material grades, is the behavior at large strains. The classical Swift law is unable to approximate the gradient at the point where extrapolation starts. The extended Swift law approximates the gradient far better and is thus considered to provide a better base for extrapolation. The best fits of the extended

Swift law for all three hardness grades are shown as the solid lines in Figure 4.

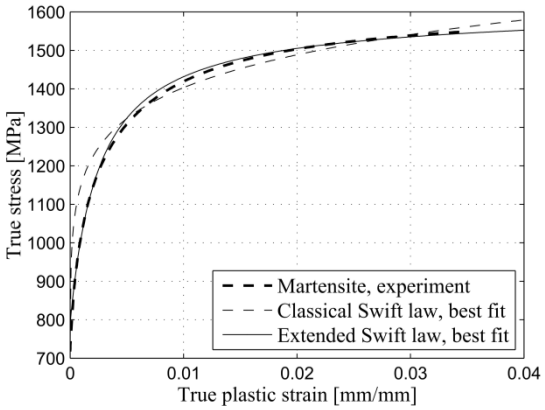

Fig. 5 *Comparison between fitted classical Swift and extended Swift hardening equations for the martensite grade.*

4.2 Fracture model

The fracture model used in this work is a strain representation of the classical Mohr-Coulomb fracture criterion, which says that fracture occurs when the combined normal stress (σ_n) and shear stress (τ) reach a critical value:

$$(\tau + c_1\sigma_n)_f = c_2 \tag{4}$$

where c_1 and c_2 are material dependent parameters. Bai [6] transformed this criterion to a strain-based form, where the equivalent strain to fracture ($\bar{\varepsilon}_f$) is defined as function of the stress triaxiality (η) and the normalized Lode angle parameter ($\bar{\theta}$). To further optimize the model for use with sheet metals, a plane stress fracture curve as established by Wierzbicki and Xue [8] is used, which allows representation of the model in $(\eta, \bar{\varepsilon}_f)$-space. The resulting fracture curves for the three 22MnB5 hardness grades are shown in Figure 6.

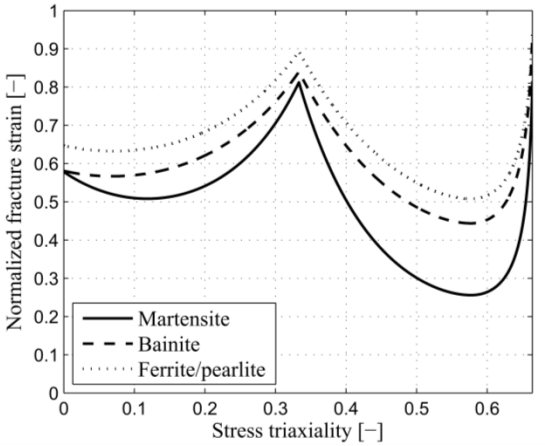

Fig. 6 *Normalized plane stress fracture curves of the three 22MnB5 hardness grades (calibrated from experiments).*

Looking at Figure 6, it can be seen that for the more ductile bainite and ferrite/pearlite grades, fracture strains are higher compared to the brittle martensite grade. Another important aspect of the three fracture curves is that there are no intersections in the calibrated range, making interpolation between them and their corresponding $(\eta, \bar{\theta}, \bar{\varepsilon}_f)$-fracture surfaces easier. It should be noted that the current strain-based fracture model is related to a specific mesh size. Especially in necking zones, where high strain gradients are found, the calculated strain field and thus the found fracture strains are highly mesh size dependent. The fracture surfaces presented in this work are calibrated to a mesh with average element edge lengths of 0.5 mm.

4.3 Hardness dependent constitutive model

Piecewise linear interpolation between the calibrated material models of the individual grades will be applied to create a model that can be used to approximate the behavior of arbitrary grades. Interpolation will take place separately for the calibrated strain hardening equations and the calibrated fracture criteria. The material hardness will be used as driving parameter. In the lower hardness range, between the experimentally determined ferrite/pearlite and bainite hardness values ($165 \leq \mathrm{HV} \leq 239$), the strain hardening and fracture behavior is described by:

$$\begin{aligned}\sigma_y(\bar{\varepsilon}_p, X_b) &= (1 - X_b) \cdot \sigma_{y,fp}(\bar{\varepsilon}_p) \\ &\quad + X_b \cdot \sigma_{y,b}(\bar{\varepsilon}_p)\end{aligned} \tag{5}$$

$$\begin{aligned}\bar{\varepsilon}_f(\eta, \bar{\theta}, X_b) &= (1 - X_b) \cdot \bar{\varepsilon}_{f,fp}(\eta, \bar{\theta}) \\ &\quad + X_b \cdot \bar{\varepsilon}_{f,b}(\eta, \bar{\theta})\end{aligned}$$

in which X_b is the proportion of bainite grade being added to the total material model. X_b is linearly related to the hardness through:

$$X_b(HV) = \frac{HV - \mathrm{HV_{fp}}}{\mathrm{HV_b} - \mathrm{HV_{fp}}} \tag{6}$$

where $\mathrm{HV_{fp}}$ and $\mathrm{HV_b}$ are the ferrite/pearlite and bainite hardness values. In the higher hardness range ($239 \leq \mathrm{HV} \leq 477$), the bainite and martensite models are mixed according to the same strategy. After implementing the model in the modular material model (MMM) framework [9] for the explicit FEM code PAM-CRASH (Virtual Performance Solution), tensile tests are simulated for several interpolated material grades, see Figure 7. Note that the value of X_b represents the fraction of bainite being added: $X_b = 1$ is a fully bainitic material, and $X_b = 0.6$ in the upper hardness range represents a mix of 60% bainite and 40% martensite. The results seem plausible, because the fracture

points all correspond to the typical strength-ductility banana shape for metals.

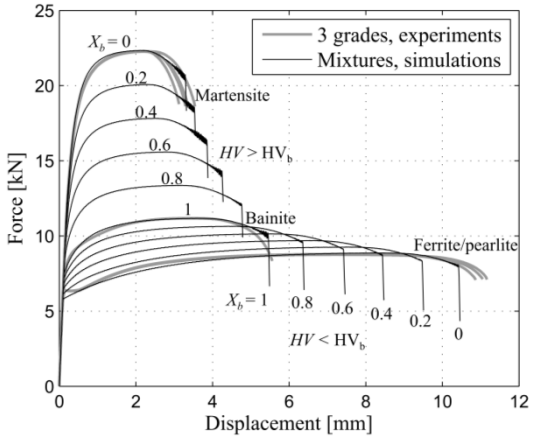

Fig. 7 *Simulation results of the standard tensile tests for several interpolated material grades.*

5 Validation with tapered tensile specimen

In order to further validate the proposed hardness dependent constitutive model, a tapered tensile test specimen with hardness transition zone in the gauge section is designed and tested. For this purpose, sheets of 22MnB5 are first fully austenitized in a furnace at 950°C, after which they are formed to top hat sections in a tailored tool. The tailored tool consists of two tool halves separated by a 1.4 mm air gap. One tool half is cooled to a temperature of 40°C, the other half is heated to 530°C. After a holding time of 20 seconds, the top hat sections are ejected and cool down to room temperature in air. Hardness measurements taken along the longitudinal axes of the top hat sections show a steep transition from 465 HV to approximately 250 HV over a range of 150 mm. Tapered tensile specimens, of which a detailed drawing is presented in Figure 8, are extracted from the top hat sections such that the hardness transition zone lies in the middle of the gauge section, see Figure 9.

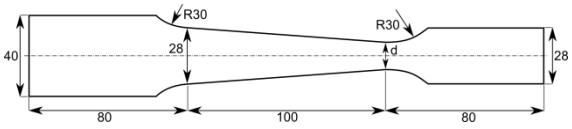

Fig. 8 *Geometry of the tapered tensile test specimen.*

If width *d* in Figure 8 would be equal to the width at the left-hand side of the specimen (28 mm), the tapered tensile specimen would reduce to a standard uni-axial tensile specimen. With a hardness transition zone in the gauge section of a standard uni-axial tensile specimen, the specimen would always neck and fail in the softest area. To avoid this trivial solution, width *d* at the right-hand side of the gauge section is reduced: the smaller width *d*, the further the necking zone moves to the right.

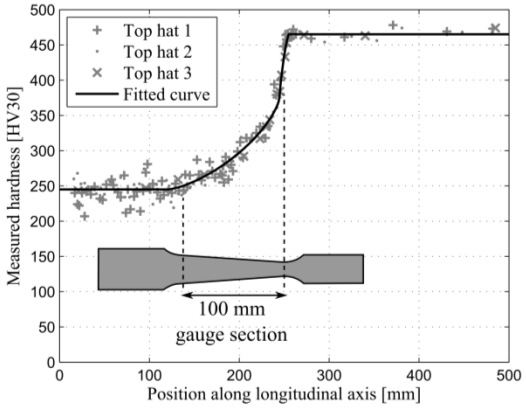

Fig. 9 *Hardness measurement results along the longitudinal axes of the top hat sections and positioning of the tapered tensile test specimen.*

Using some preliminary simulations, two values of *d* are chosen such that the necking area lies safely within the boundaries of the gauge section: d = 14 mm and d = 18 mm. The resulting force-displacement curves are presented in Figure 10.

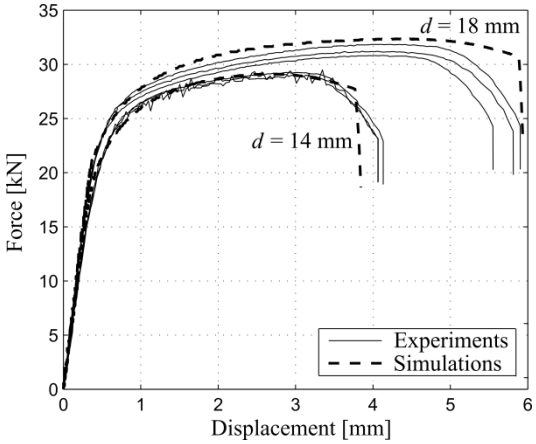

Fig. 10 *Force-displacement results of the tapered tensile test specimens.*

Three experiments have been performed for each value of *d* and confirmed excellent repeatability considering both the fracture location and the force-displacement curves. The simulated force-displacement curves are shown in Figure 10 as well. It can be seen that the newly developed model predicts the experimental curves with good accuracy, both for the narrow and the wide specimen.

6 CONCLUSIONS

Three hardness grades of quench-hardenable boron steel 22MnB5 have been used to calibrate a hardness dependent constitutive model consisting of an extended Swift hardening law and a stress triaxiality and Lode angle dependent fracture criterion.

Piecewise linear interpolation between the calibrated grades was applied to obtain a model for arbitrary grades.
Simulations of standard tensile tests with some selected hardness values showed that the model provides plausible results. For further validation, a newly developed tapered tensile test specimen was used featuring a hardness transition in the gauge section. The experiments showed excellent repeatability considering both the fracture location and the force-displacement curves, which were approximated by the simulation model with good accuracy.

7 ACKNOWLEDGEMENT

The authors thank Dr. H.J.M. Geijselaers from the University of Twente for the valuable discussions on phase transformation kinetics. Thanks are due to G. Wuttke and M. Stanke from VW Group Research for their support during the experimental part of this work.

REFERENCES

[1] Maikranz-Valentin M., Weidig U., Schoof U., Becker H. H., Steinhoff K. *Components with optimised properties due to advanced thermomechanical process strategies in hot sheet metal forming*. Steel research international 79(2):92-97, 2008.
[2] George R., Bardelcik A., Worswick M. J.: *Hot forming of boron steels using heated and cooled tooling for tailored properties*. Journal of Materials Processing Technology, 212(11):2386-2399, 2012.
[3] ArcelorMittal. *Steels for hot stamping*. Product catalog, 2012.
[4] ArcelorMittal. *A54 - quenchable boron steels*. Product catalog, 2011.
[5] ArcelorMittal. *Personal communication with ArcelorMittal.*
[6] Bai, Y. *Effect of Loading History on Necking and Fracture.* Ph.D. thesis, Massachusetts institute of technology, MA, 2008.
[7] Eller T. K., Greve L., Andres M. T., Medricky M., Hatscher A., Meinders V. T., Van den Boogaard A. H. *Plasticity and fracture modeling of quench-hardenable boron steel with tailored properties.* Submitted to Journal of Material Processing Technology, 2013.
[8] Wierzbicki T., Xue L. *On the effect of the third invariant of the stress deviator on ductile fracture*. Technical Report, Massachusetts institute of technology, MA, 2005.
[9] Greve L. *Modulare Materialmodellierung für die Simulation von Deformations- und Bruchvorgängen.* Presented at crashMAT 2012 - 6. Freiburg Workshop zum Werkstoff- und Strukturverhalten bei Crashvorgängen, 2012.